CONTROL AND OPERATION OF A DC GRID-BASED WIND POWER GENERATION SYSTEM IN A MICROGRID

[1]K V.S SUBRAHMANYAM, [2]D.RAMU

[1]M.Tech, NOVA INSTITUTE OF ENGINEERING AND TECHNOLOGY, VEGAVARAM, JANGAREDDYGUDEM, AP
[2]Associate Professor, NOVA INSTITUTE OF ENGINEERING AND TECHNOLOGY, VEGAVARAM, JANGAREDDYGUDEM, AP

ABSTRACT- This paper presents the control and operation of a dc grid-based wind power generation system in a poultry farm. In This method voltage and frequency synchronization elimination is done by allowing the flexible operation of multiple parallel-connected wind generators. A model predictive control algorithm that offers better transient response with respect to the changes in the operating conditions is proposed for the control of the inverters. The design concept is verified through various test scenarios to demonstrate the operational capability of the proposed microgrid when it operates connected to and islanded from the distribution grid and the results are simulated in the MATLAB-SIMULINK.

I. INTRODUCTION

Many trends are becoming noticeable that will change the requirements of energy delivery. These modifications are being driven from both the demand and supply side where the integration of distributed generation and peak shaving technologies must be accommodated. Generally more than 90% of low voltage domestic customers are supplied by underground cable when the reset is supplied by overhead lines. The micro grid often supplies both electricity and heat to the customer by means of combined heat and power plants (CHP), gas turbines, fuel cells, photovoltaic (PV) systems, wind turbines, etc. The energy storage systems usually include batteries and flywheels .

The storing device in the micro grid is equivalent to the rotating reserve of large generators in the conventional grid which ensures the balance between energy generation and consumption during rapid changes in load or generation. The development of micro grids can contribute to the reduction of emissions and the mitigation climate changes. This is due to the availability and developing technologies for distributed generation units are based on the renewable sources and micro sources that are characterized by very low emissions. Protection system is one of the major challenges for micro grid which must react to both main grid and micro grid faults.

The protection system should cut off the micro grid from the main grid as rapidly as necessary to protect the micro grid loads for the first case and second case the protection system should isolate the smallest part of the micro grid when clears the faults . Micro grids have large power capacity and more control flexibility which accomplishes the reliability of the system as well as the requirement of power quality. Operation of micro grid needs implementation of high performance power control regulation algorithm. To realize the emerging potential of distributed generation, a system approach i.e. micro grid is proposed which considers of generation and associated loads as a subsystem. This approach involves local control of distributed generation and hence reduces the need for central dispatch. During disturbances by islanding generation and loads, local reliability can be higher in micro grid than the whole power system. The micro grid concept lowers the cost and improves the reliability of small scale distributed generators.

The main purpose of this concept is to accelerate the recognition of the advantage offered by small scale distributed generators like ability to supply waste heat during the time need. This concept permits high penetration of distribution generation without requiring redesign of the distribution system itself. The micro grid concept acts as solution to the problem of integrating large amount of micro generation without interrupting the utility networks operation. The micro grid or distribution network subsystem will create less trouble to the utility network than the conventional micro generation if there is proper and intelligent coordination of micro generation and loads. In case of disturbances on the main network, micro grid could potentially disconnect and continue to operate individually, which helps in improving power quality to the consumer.

II. SYSTEM DESCRIPTION AND MODELING

A. System Description

The general configuration of the proposed dc grid based wind power generation system for the poultry cultivate is appeared in Fig. 1. The system can work either associated with or islanded from the distribution grid and comprises of four 10 kW

changeless magnet synchronous generators (PMSGs) which are driven by the variable speed WTs. The three-phase output of each PMSG is associated with a three-phase converter (i.e., converters A, B, C and D), which works as a rectifier to direct the dc output voltage of each PMSG to the coveted level at the dc grid.

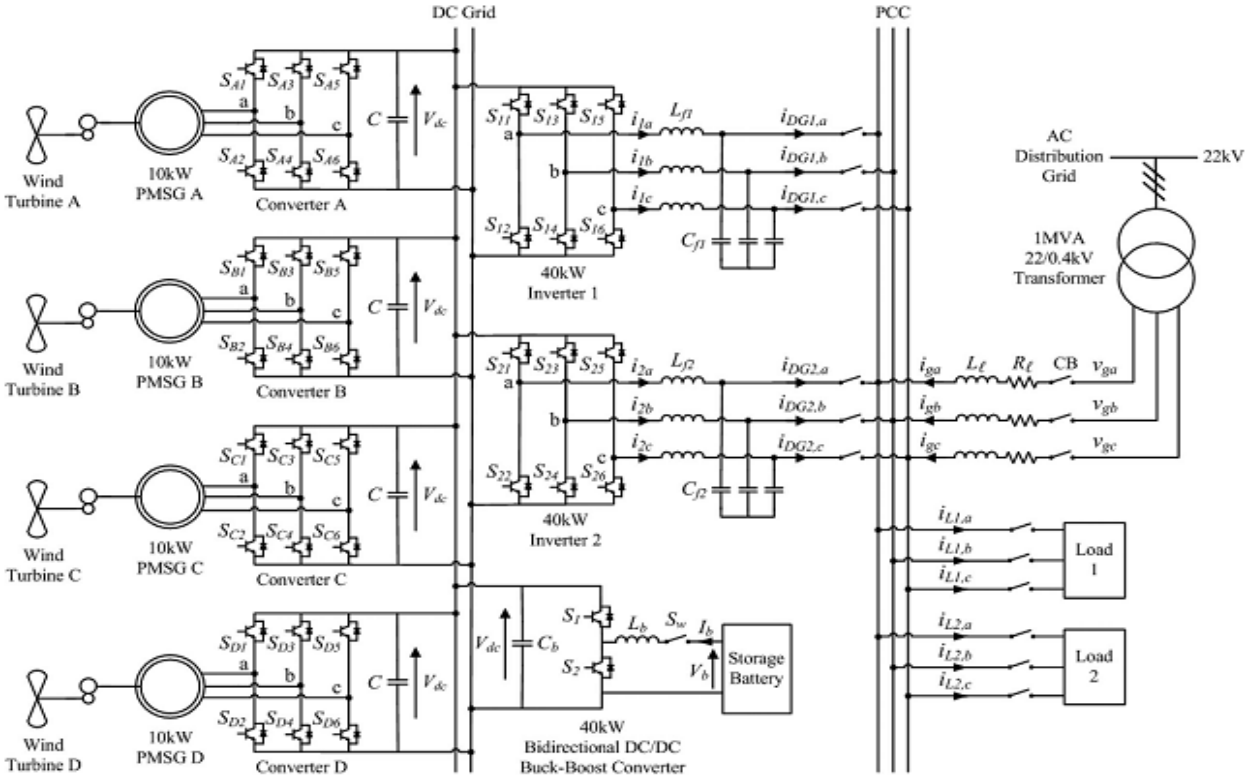

Fig.1. Overall configuration of the proposed dc grid based wind power generation system in a micro grid

This engineering limits the need to synchronize the frequency, voltage and phase, decreases the requirement for numerous inverters at the generation side, and gives the adaptability to the fitting and play association of WGs to the dc grid. The accessibility of the dc grid will likewise empower the supply of power to dc loads all the more productively by lessening another air conditioner/dc change. The coordination of the converters and inverters is accomplished through a brought together energy administration system (EMS). The EMS controls and screens the power dispatch by each WG and the load power utilization in the microgrid through a concentrated server. To avert exorbitant circulating currents between the inverters, the inverter output voltages of inverters 1 and 2 are directed to a similar voltage. Through the EMS, the output voltages of inverters 1 and 2 are constantly observed to guarantee that the inverters maintain similar output voltages.

Amid ordinary operation, the two inverters will share the maximum output from the PMSGs (i.e., every inverter shares 20 kW). The maximum power produced by each WT is evaluated from the ideal wind power $P_{wt,opt}$ as takes after [23]:

$$P_{wt,opt} = k_{opt}\left(w_{r,opt}\right)^3 \quad (1)$$

$$k_{opt} = 0.5 C_{p,opt} \rho A \left(\frac{R}{\lambda_{opt}}\right)^3 \quad (2)$$

$$w_{opt} = \left(\frac{\lambda_{opt}}{R}\right) \quad (3)$$

where k select is the upgraded constant, ωr, opt is the WT speed for ideal power generation, Cp, pick is the ideal power coefficient of the turbine, ρ is the air thickness, An is the zone cleared by the rotor edges, λ_{opt} is the ideal tip speed ratio, v is the wind speed and R is the range of the edge. When one inverter neglects to work or is under maintenance, the other inverter can deal with the maximum power output of 40 kW from the PMSGs. The energy requirements of the SB in the proposed dc grid are resolved based on the system-on-a-chip (SOC) limits given by

$$SOC_{min} < SOC \leq SOC_{max} \quad (4)$$

B. System Operation

At the point when the microgrid is working associated with the distribution grid, the WTs in the micro grid are in charge of giving neighborhood power support to the loads, along these lines diminishing the weight of power conveyed from the grid. The SB can be controlled to accomplish distinctive request side administration functions, for example, crest shaving and valley filling relying upon the time-of-utilization of power and SOC of the SB. Amid islanded operation where the CBs detach the micro grid from the distribution grid, the WTs and the SB are just accessible sources to supply the load request. The SB can supply for the shortfall in genuine power to maintain the power adjust of the micro grid as takes after:

$$P_{wt} + P_{sb} = P_{loss} + P_l \quad (5)$$

Where P_{wt} is the genuine power created by the WTs, P_{sb} is the genuine power provided by SB which is subjected to the requirement of the SB maximum power P_{sb}, max that can be conveyed amid releasing and is given by

$$P_{sb} \leq P_{sb,max} \quad (6)$$

P_{loss} is the system misfortune, and fuzzy is the real power that is provided to the loads

C. AC/DC Converter Modeling

Fig. 2 demonstrates the power circuit comprising of a PMSG which is associated with an air conditioner/dc voltage source converter. The PMSG is displayed as an adjusted three-phase air conditioning voltage source e_{sa}, e_{sb}, e_{sc} with series obstruction R s and inductance Ls. As appeared in, the state conditions for the PMSG currents i_{sa}, i_{sb}, i_{sc} and the dc output voltage V_{dc} of the converter can be communicated as takes after:

$$L_s \frac{di_s}{dt} = -R_s L_s + e_s - KSV_{dc} \quad (7)$$

$$C = \frac{dV_{dc}}{dt} = i_s{}^T S - I_{dc} \quad (8)$$

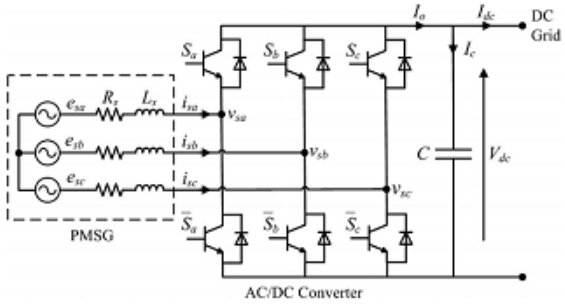

Fig.2. Power circuit of a PMSG connected to an ac/dc voltage source converter.

Where

$$i_s = [i_{sa} \quad i_{sb} \quad i_{sc}]^T, e_s = [e_{sa} \quad e_{sb} \quad e_{sc}]^T$$

$$K = \begin{bmatrix} 2/3 & -1/3 & -1/3 \\ -1/3 & 2/3 & -1/3 \\ -1/3 & -1/3 & 2/3 \end{bmatrix}$$

$S = [S_a \quad S_b \quad S_c]^T$ is the ac/dc converter switching functions which are defined as

$$S_j = \begin{cases} 1, & S_j \ is \ ON \\ 0 & S_j \ is \ OFF \end{cases} \quad \text{For j= a, b, c} \quad (9)$$

D. DC/AC Inverter Modeling

The two 40 kW three-phase dc/air conditioning inverters which interface the dc grid to the point of regular coupling (PCC) are indistinguishable, and the single-phase portrayal of the three-phase dc/air conditioning inverter is appeared in Fig. 3. To determine a state-space demonstrate for the inverter, Kirchhoff's voltage and current laws are connected to circle I and point x separately, and the accompanying conditions are acquired:

$$L_f \frac{di}{dt} + iR + v_{dc} = uV_{dc} \quad (10)$$

$$i_{DG} = i - i_{Cf} \quad (11)$$

where V_{dc} is the dc grid voltage, u is the control signal, R is the inverter misfortune, L_f and C_f are the inductance and capacitance of the low-pass (LPF) filter separately, i_{DG} is the inverter output current, I is the present flowing through Lf , i_{Cf} is the present flowing through C_f , and v_{DG} is the inverter output voltage.

Along these lines, the discrete state-space conditions for the inverter show working in the CCM can be communicated with examining time Ts as takes after:

$$x_g(k+1) = A_g x_g(k) + B_{g1} v_g(k) + B_{g2} u_g(k) \quad (12)$$

$$y_g(k) = C_g x_g(k) + D_g v_g(k) \quad (13)$$

Where the subscript g represents the inverter model during grid connected operation, k is the discredited present time step, and

$$A_g = 1 - \frac{R}{L_f} T_S, \quad B_{g1} = \left[0 \quad -\frac{T_S}{L_f}\right],$$

$$B_{g2} = \frac{v_{dc}}{L_f}, C_g = 1, \ D_g = \left[\frac{C_f}{T_S} \quad -\frac{C_f}{T_S}\right]$$

x g(k) = i(k) is the state vector; vg(k) = [vDG(k + 1) vDG(k)]T is the exogenous input; $u_g(k)$ is the control signal with $-1 \leq u_g(k) \leq 1$; and $y_g(k)$ = iDG(k) is the output. The exogenous input $v_g(k)$ can be calculated using state estimation.

The voltage of the PCC will be maintained by the inverters when the microgrid is islanded from the grid. When contrasted with Ts, the rate of progress of the inverter output current is much slower. In this way, the accompanying presumption is made when determining the state-space conditions for the inverter working in the VCM:

$$\frac{di_{DG}}{dt} = 0 \quad (14)$$

Based on the previously mentioned supposition, the discrete state space conditions of the inverter demonstrate working in the VCM can be communicated as takes after

$$x_i(k+1) = A_i x_i(k) + B_i u_i(k) \quad (15)$$

$$y_i(k) = C_i x_i(k) \quad (16)$$

where the subscript I speaks to the model of the inverter amid islanded operation and $x_i(k) = [i(k)\ v_{DG}(k)\ i_{DG}(k)]T$ is the state vector; $u_i(k)$ is the control signal with $-1 \le u_i(k) \le 1$; and $y_i(k) = vDG(k)$ is the output. Amid islanded operation, the inverters are required to convey all the accessible power from the PMSGs to the loads. In this manner, just the inverter output voltage is controlled and the output current is resolved from the measure of accessible power.

III. CONTROL DESIGN

A. Control Design for the AC/DC Converter

Fig. 3 demonstrates the configuration of the proposed controller for every air conditioner/dc voltage source converter which is utilized to maintain the dc output voltage Vdc of every converter and adjust for any variety in Vdc because of any power lopsidedness in the dc grid. The power unevenness will actuate a voltage mistake ($V_{dc}^* - V_{dc}$) at the dc grid, which is then encouraged into a corresponding essential controller to produce a present reference i^*_d for id to track. To dispense with the nearness of high frequency switching swells at the dc grid, Vdc is first gone through a first-arrange LPF. The present I q is controlled to be zero so the PMSG just conveys genuine power. The present mistakes Δi_d and Δi_q are then changed over into the abc casing and nourished into a relative resounding (PR) controller to produce the required control signals utilizing pulse-width tweak.

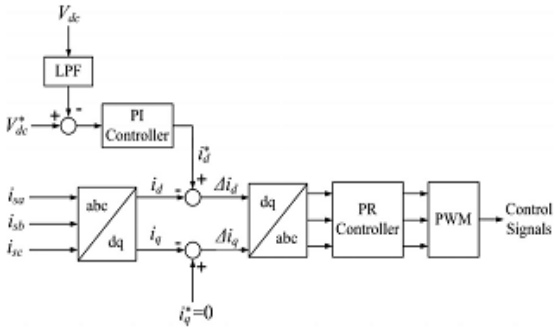

Fig.3.Configuration of the proposed controller for the ac/dc converter

B. Control Design for the DC/AC Inverter

All together for the microgrid to work in both grid-associated and islanded methods of operation, a model-based controller utilizing MPC is proposed for the control of the inverters. MPC is a model-based controller and embraces a retreating skyline approach in which the enhancement calculation will figure a sequence of control activities to limit the chose goals for the entire control skyline, yet just execute the principal control activity for the inverter. At whenever step, the enhancement procedure is rehashed based on new estimations over a moved forecast skyline. To determine the control calculation for the inverters, the state-space conditions are changed into increased state-space conditions by characterizing the incremental variables in the accompanying organization:

$$\Delta\xi(k) = \xi(k) - \xi(k-1) \quad (17)$$

Where ξ speaks to every variable in the inverter display, for example, v_{DG}, i_{DG}, I and u as appeared in Fig. 4. By characterizing the incremental variables, the enlarged state space show for the inverter display working in the CCM amid grid-associated operation can be communicated as takes after:

$$x_g(k+1) = A_{g\_aug}X_g(k) + B_{g1\_aug}V_g(k) + B_{g2\_aug}U_g(k) \quad (18)$$

$$Y_g(k) = C_{g_{aug}}X_g(k) \quad (19)$$

Additionally, the increased state-space display for the inverter demonstrates working in the VCM amid islanded operation can be communicated as takes after:

$$X_i(k+1) = A_{i\_aug}X_i(k) + B_{i\_aug}U_i(k) \quad (20)$$

$$Y_i(k) = C_{i\_aug}X_i(k) \quad (21)$$

Where

$X_i(k) = [\Delta_i(k)\ \Delta V_{DG}(k)\ \Delta i_{DG}(k)\ v_{DG}(k)]^T$ is the state vector; $U_i(k) = \Delta u_i(k)$ is the control signal; and $Y_i(k) = v_{DG}(k)$ is the output. For the control of the two augmented models in the CCM and the VCM, the following cost function is solved using quadratic programming in the proposed MPC algorithm.

$$J = (R_s - Y_j)^T + U_j{}^T Q U_j \quad (22)$$

After the control signal u is created by the MPC calculation, it will be connected to the dc/air conditioning inverter as appeared in Fig. 4.the MATLAB circuit for dc/air conditioning inverter control utilizing PI controller is appeared in fig 5.

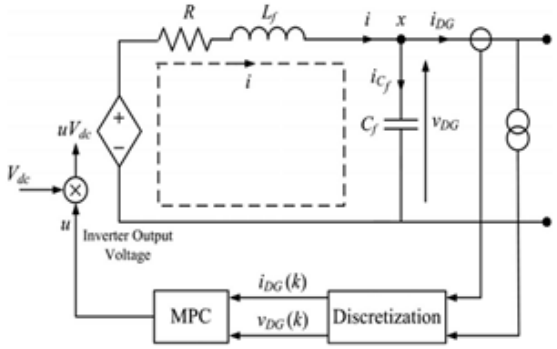

Fig.4. Single-phase representation of the three-phase dc/ac inverter

IV. NUMERICAL SIMULATION ANALYSIS

The simulation model of the proposed dc grid based wind power generation system shown in Fig. 1 is implemented in MATLAB/Simulink. The effectiveness of the proposed design concept is evaluated under different operating conditions when

the microgrid is operating in the grid-connected or islanded mode of operation. The system parameters are given in Table I. The impedances of the distribution line are obtained from. In practical implementations, the values of the converter and inverter loss resistance are not precisely known. Therefore, these values have been coarsely estimated.

TABLE I
PARAMETERS OF THE PROPOSED SYSTEM

Parameter	value
Distribution grid voltage	$v_g = 230V\ (Phase)$
Dc grid voltage	$V_{dc} = 500V$
PMSG stator impedance	$R_s = 0.2\Omega, L_s = 2.4mH$
Distribution line impedance	$R_l = 7.5m\Omega, L_l = 25.7\mu H$
Inverter LC filter	$L_f = 1.2mH, C_f = 20\mu F$
Converter capacitor	C=300 μF
Converter and inverter loss resistance	R=1mΩ
Load 1 rating	$P_{L1} = 35kW, Q_{L1} = 8kVAr$
Load 2 rating	$P_{L2} = 25kW, Q_{L2} = 4kVAr$

Test Case 1: Failure of One Inverter during Grid-Connected Operation

When one of the inverters fails to operate and needs to be disconnected from the dc grid, the other inverter is required to handle all the power generated by the PMSGs. In this test case, an analysis on the microgrid operation when one of the inverters is disconnected from operation is conducted.

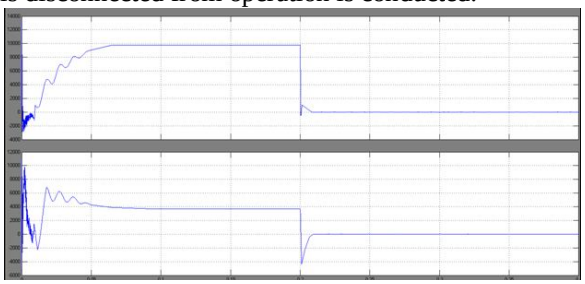

Fig.5. Real (top) and reactive (bottom) power delivered by inverter 1

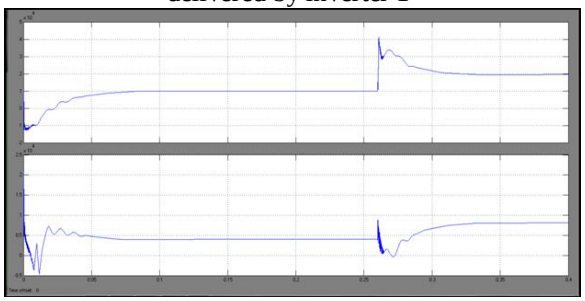

Fig.6. Real (top) and reactive (bottom) power delivered by inverter 2

Figs. 5 and 6 show the waveforms of the real and reactive power delivered by inverters 1 and 2 for $0 \leq t < 0.4$ s respectively. For $0 \leq t < 0.2$ s, both inverters 1 and 2 are in operation and each inverter delivers about 10 kW of real power and 4 kVAr of reactive power to the loads.

The remaining real and reactive power that is demanded by the loads is supplied by the grid which is shown in Fig.7. It can be seen from Fig. 7 that the grid delivers 40 kW of real power and 4 kVAr of reactive power to the loads for $0 \leq t < 0.2$ s.

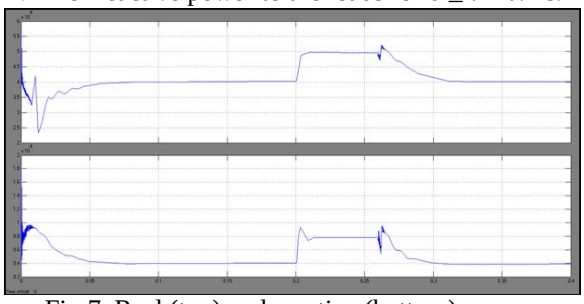

Fig.7. Real (top) and reactive (bottom) power delivered by the grid

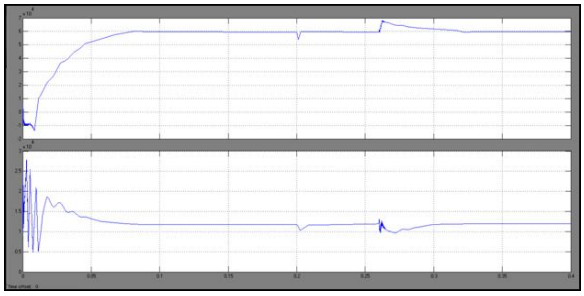

Fig.8. Real (top) and reactive (bottom) power consumed by the loads

This undelivered power causes a sudden power surge in the dc grid which corresponds to a voltage rise at t = 0.2 s as shown in Fig. 8.

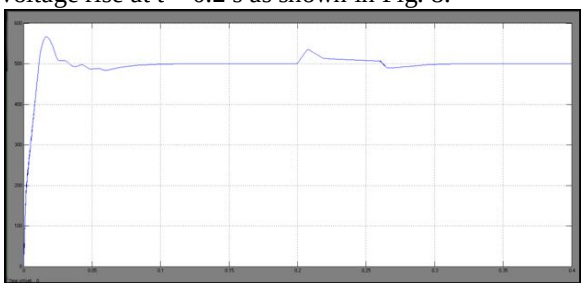

Fig.9. DC grid voltage

It is observed from Fig. 8 that the voltage at the dc grid corresponds to a voltage dip at t = 0.26 s due to the increase in power drawn by inverter 2 and then returns to its nominal value of 500 V for $0.26 \leq t < 0.4$ s. As observed in Fig. 8, at t = 0.26 s, the changes in power delivered by inverter 2 and the grid also cause a transient in the load power.

Test Case 2: Connection of AC/DC Converter during Grid-Connected Operation

The real power generated from each of the remaining three PMSGs is maintained at 5.5 kW and their aggregated real power of 16.5 kW at the dc grid

is converted by inverters 1 and 2 into 14 kW of real power and 8 kVAr of reactive power. As shown in Figs. 10 and 11, each inverter delivers real and reactive power of 7 kW and 4 kVAr to the loads respectively. The rest of the real and reactive power demand of the loads is supplied by the grid as shown in Fig. 12.

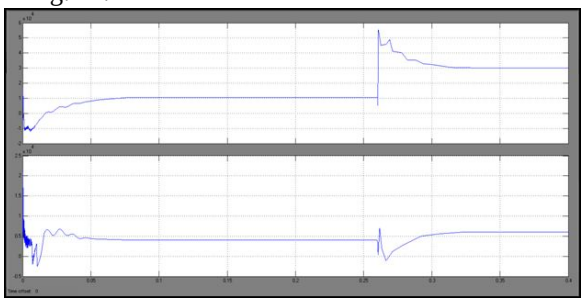

Fig.10. Real (top) and reactive (bottom) power delivered by inverter 1

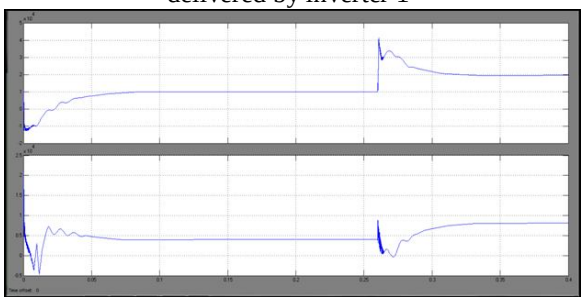

Fig.11. Real (top) and reactive (bottom) power delivered by inverter 2

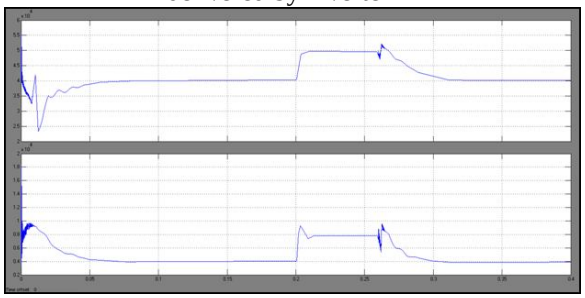

Fig.12. Real (top) and reactive (bottom) power delivered by the grid

It can be seen from Fig. 12 that the grid delivers 46 kW of real power and 4 kVAr of reactive power to the loads. At t = 0.2 s, PMSG A which generates real power of 5.5 kW is connected to the dc grid. This causes a sudden power surge at the dc grid and results in a voltage rise at t = 0.2 s as shown in the voltage waveform of Fig. 13. At t = 0.26 s, the EMS increases the real delivered by each inverter to 10 kW while the reactive power supplied by each inverter remains unchanged at 4 kVAr as shown in Figs. 15 and 16.

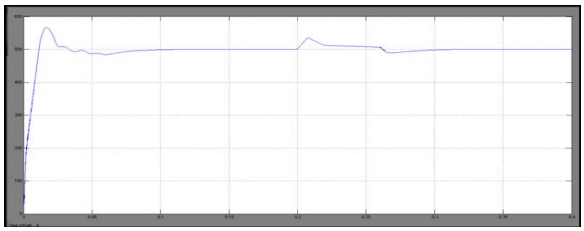

Fig.13. DC grid voltage

The grid also simultaneously decreases its supply to 40 kW of real power for $0.26 \leq t < 0.4$ s while its reactive power remains constant at 4 kVAr as shown in Fig. 12.

Test Case 3: Islanded Operation When the microgrid operates islanded from the distribution grid, the total generation from the PMSGs will be insufficient to supply for all the load demand.

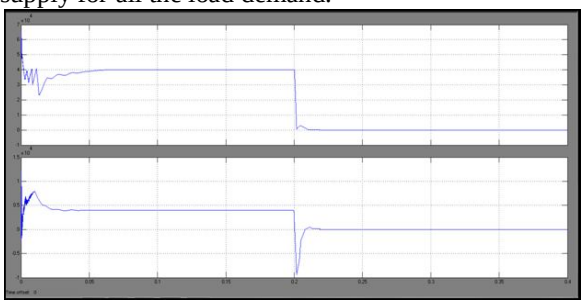

Fig.14. Real (top) and reactive (bottom) power delivered by the grid

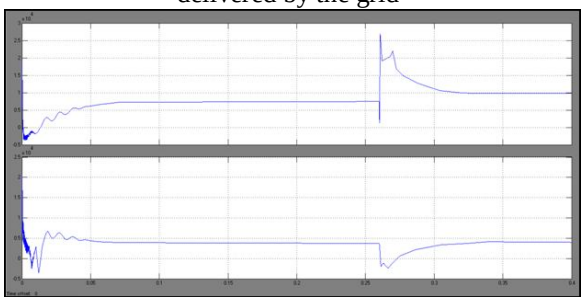

Fig.15. Real (top) and reactive (bottom) power delivered by inverter 1

The microgrid is initially operating in the grid-connected mode. The grid is supplying real power of 40 kW and reactive power of 4 kVAr to the loads for $0 \leq t < 0.2$ s as shown in Fig. 14 while each inverter is delivering real power of 10 kW and reactive power of 4 kVAr to the loads as shown in Figs. 15 and 16. At t = 0.2 s, the microgrid is disconnected from the distribution grid by the CBs due to a fault occurring in the upstream network of the distribution grid.

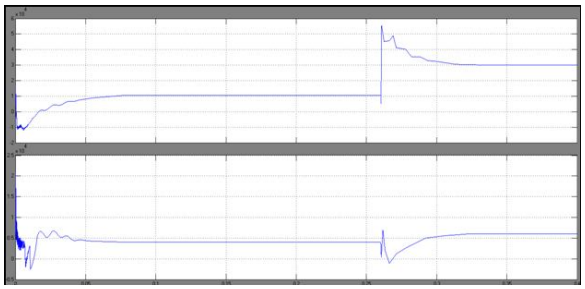

Fig.16. Real (top) and reactive (bottom) power delivered by inverter 2

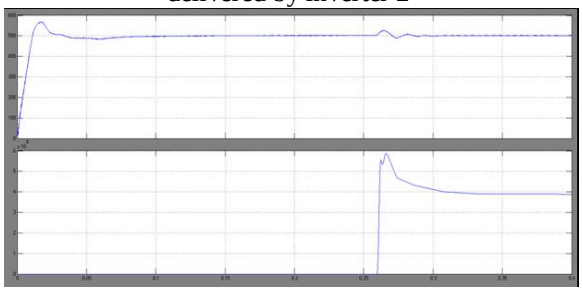

Fig.17. DC grid voltage and Real power delivered by SB

At the same time, the real and reactive power delivered by each inverter is also increased by the EMS to 30 kW and 6 kVAr as shown in Figs. 15 and 16 respectively. Fig. 17 shows the dc grid voltage where slight voltage fluctuations are observed at t = 0.26 s.

V. CONCLUSION

The design of dc grid based wind power generation system in a microgrid using, is proposed in this paper that enables parallel operation of several WGS in a poultry farm. As we compare to traditional wind power generation systems, the proposed system design with mitigates the need for voltage and frequency synchronization, it will allows the WGs to be switched on or off with minimal disturbances to the microgrid operation. The simulation results obtained and the analysis performed in this paper serve as a basis for the design of a dc grid based wind power generation system in a microgrid.

REFERENCES

[1] M. Czarick and J. Worley, “Wind turbines and tunnel fans,” Poultry Housing Tips, vol. 22, no. 7, pp. 1–2, Jun. 2010.

[2] The poultry guide: Environmentally control poultry farm ventilation systems for broiler, layer, breeders and top suppliers. [Online]. Available: http://thepoultryguide.com/poultry-ventilation/

[3] Livestock and climate change. [Online]. Available: http://www. worldwatch.org /files/pdf/ Livestock%20and%20Climate%20Change.pdf.

[4] Farm Energy: Energy efficient fans for poultry production. [Online]. Available: http://farmenergy.exnet.iastate.edu.

[5] A. Mogstad, M. Molinas, P. Olsen, and R. Nilsen, “A power conversion system for offshore wind parks,” in Proc. 34th IEEE Ind. Electron., 2008, pp. 2106–2112

. [6] A. Mogstad and M. Molinas, “Power collection and integration on the electric grid from offshore wind parks,” in Proc. Nordic Workshop Power Ind. Electron., 2008, pp. 1–8. [7] D. Jovic, “Offshore wind farm with a series multiterminal CSI HVDC,” Elect. Power Syst. Res., vol. 78, no. 4, pp. 747–755, Apr. 2008.

[8] X. Lu, J. M. Guerrero, K. Sun, and J. C Vasquez “An improved droop control method for DC microgrids based on low bandwidth communication with DC bus voltage restoration and enhanced current sharing accuracy,” IEEE Trans. Power Electron., vol. 29, no. 4, pp. 1800–1812, Apr. 2014.

[9] T. Dragicevi, J. M. Guerrero, and J. C Vasquez, “A distributed control strategy for coordination of an autonomous LVDC microgrid based on power-line signaling,” IEEE Trans. Ind. Electron., vol. 61, no. 7, pp. 3313–3326, Jul. 2014.

[10] N. L. Diaz, T. Dragicevi, J. C. Vasquez, and J. M. Guerrero, “Intelligent distributed generation and storage units for DC microgrids—A new concept on cooperative control without communications beyond droop control,” IEEE Trans. Smart Grid, vol. 5, no. 5, pp. 2476–2485, Sep. 2014.

[11] T.-S. Lee, K.-S. Tee and M.-S. Chong, “Fuzzy iterative learning control for three phase shunt active power filter,” IEEE Inter. Symp. On Ind. Elec., pp. 882-885, ISIE 2006, Canada.

[12] X. Dianguo, H. Na, W. Wei, “Study on fuzzy controller with a self-adjustable factor of active power filter,” 32nd Annual Conf. of the IEEE Industrial Elec. Society, pp. 2226-2231, IECON 2006 (PDF) Adaptive Control of Shunt Active Power Filter Using Interval Type-2 Fuzzy Logic Controller.